Reduction Kinetics of Graphene Oxide Determined by Electrical Transport Measurements and Temperature Programmed Desorption

Inhwa Jung,[†] Daniel A. Field,[‡] Nicholas J. Clark,[‡] Yanwu Zhu,[†] Dongxing Yang,[†] Richard D. Piner,[†] Sasha Stankovich,[§] Dmitriy A. Dikin,[§] Heike Geisler,[||] Carl A. Ventrice, Jr.,*,[‡] and Rodney S. Ruoff*,[†]

Department of Mechanical Engineering and the Texas Materials Institute, University of Texas at Austin, Austin, Texas, 78712, Department of Physics, Texas State University, San Marcos, Texas, 78666, Department of Mechanical Engineering, Northwestern University, Evanston, Illinois, 60208, and Insitute for Environmental and Industrial Science, Texas State University, San Marcos, Texas, 78666

The thermal stability and reduction kinetics of graphene oxide were studied by measuring the electrical resistivity of single-layer graphene films at various stages of reduction in high vacuum and by performing temperature programmed desorption (TPD) measurements of multilayer films in ultrahigh vacuum. The graphene oxide was exfoliated from the graphite oxide source material by slow-stirring in aqueous solution, which produces single-layer platelets with an average lateral size of ∼10 μm. From the TPD measurements, it was determined that the primary desorption products of the graphene oxide films for temperatures up to 300 °C are H_2O, CO_2, and CO, with only trace amounts of O_2 being detected. Resistivity measurements on individual single-layer graphene oxide platelets resulted in an activation energy of 37 ± 1 kcal/mol. The TPD measurements of multilayer films of graphene oxide platelets give an activation energy of 32 ± 4 kcal/mol.

1. Introduction

Graphene oxide, which is an electrical insulator, shows promise for use in several technological applications. For instance, individual, monolayer, graphene oxide platelets could be used as dielectric layers in nanoscale electronic devices. Since the electrical, optical, and mechanical properties of graphene oxide can be controlled by chemical modification, films composed of layers of graphene oxide platelets may be used as the active region of chemical sensors.[1−4] In principle, graphene oxide films could also be used as a precursor for the formation of large-scale graphene films by either thermal or chemical reduction of the graphene oxide.[5−11]

Graphene oxide is formed by extensive chemical oxidation of graphite to form graphite oxide[12−14] followed by exfoliation to monolayer thick platelets by techniques such as sonication[6,15,16] or slow-stirring in aqueous solution.[11] It is a nonstoichiometric compound; therefore, the carbon-to-oxygen (C/O) ratio depends on the method of preparation and by how much the material is reduced. Previous measurements of the C/O ratio of graphene oxide films by X-ray photoelectron spectroscopy (XPS) have determined that the ratio of fully oxidized graphene oxide is 2:1.[17] The geometric structure of fully oxidized graphene oxide is still an open question. Several different models have been proposed, with some of these models predicting a planar structure,[18,19] while others favor a buckled structure.[17,20−22] Although there is general agreement that the chemical composition of graphene oxide is primarily carbon, oxygen, and hydrogen, the assignment and positions of the functional groups

of the oxide are still debated. Some of the functional groups proposed to exist at the surfaces of graphene oxide are epoxide (C−O−C), single-bonded on-top oxygen (C−O), and hydroxyl (C−OH) groups. In addition, carbonyl (C=O) groups are expected to form at missing carbon atom defect sites of the surface, and carboxylic (O=C−OH) groups, carbonyl groups, and hydroxyl groups are expected to form on the edges of the platelets. Recent solid-state NMR studies of ^{13}C-labeled graphite oxide have shed further light on this topic.[23]

Before graphene oxide can be used in most technological applications, it is important to understand its thermal stability and reduction kinetics. For instance, the decomposition temperature of graphene oxide will govern which processing techniques can be used to manufacture nanoscale electronic devices and sensors based on this material. Despite the potential technological importance of this material, there have been relatively few studies of the thermal stability of either graphite oxide[5,24,25] or graphene oxide.[7,11,26,27] An early study of the thermal decomposition of graphite oxide using gas chromatography found that the primary desorption products are H_2O, CO_2, and CO and that the decomposition occurs over a temperature range of 80−180 °C.[24] These results indicate that graphene oxide is a rather fragile material and that since there is carbon loss upon reduction, the structural integrity of the carbon backbone of the graphene will most likely be compromised upon decomposition. In fact, evidence for the generation of holes in thermally expanded graphite oxide has been discussed previously.[28]

In this study, the reaction kinetics and reduction process of graphene oxide films have been investigated using two techniques: monitoring the resistivity of a single-layer platelet of graphene oxide at various stages of reduction in high vacuum, and temperature programmed desorption (TPD) measurements of multilayer films under ultrahigh vacuum (UHV) conditions.
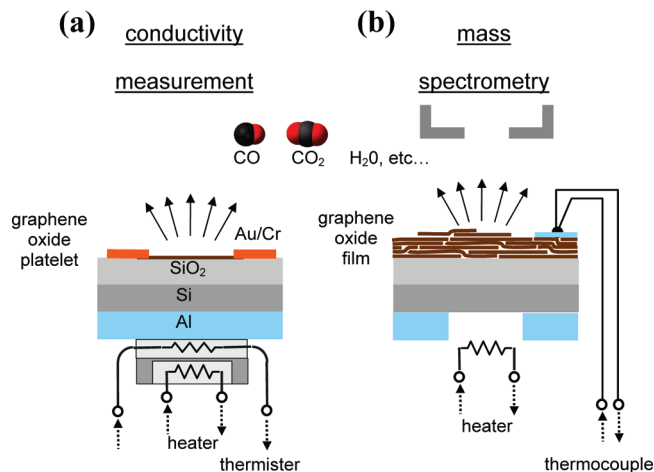
* To whom correspondence should be addressed. E-mail: cventrice@ txstate.edu (C.A.V.); r.ruoff@mail.utexas.edu (R.S.R.).
† University of Texas at Austin.
‡ Department of Physics, Texas State University.
§ Northwestern University.
|| Institute for Environmental and Industrial Science, Texas State University.

Reduction Kinetics of Graphene Oxide

*J. Phys. Chem. C, Vol. 113, No. 43, 2009* **18481**

Figure 1. Schematic of the experimental setup for (a) the resistivity measurements of an individual single-layer graphene oxide platelet and (b) the TPD measurements of multilayer graphene oxide films.

A schematic of these two techniques is shown in Figure 1. For the first method, the resistivity is monitored at constant temperature as a function of time and is then repeated for different temperatures ranging from 140 to 200 °C. From the time dependence of the resistivity, the reaction order, rate constant, and an estimated value of activation energy are acquired. From the TPD measurements, the relative coverage of the desorption products is determined by analyzing the areas under the partial pressure versus time curves. In addition, activation energies for decomposition of the oxide are determined with TPD by measuring the shift of the temperature at which the maximum of the partial pressure versus temperature plot occurs (T_M) as the heating rate (β) of the sample is increased. From the TPD measurements, it is determined that the primary desorption products of the graphene oxide films for temperatures up to 300 °C are H_2O, CO_2, and CO, with a similar T_M for all three molecular species. Activation energies of 37 ± 1 and 32 ± 4 kcal/mol are measured by resistivity measurements on single-layer graphene oxide and TPD measurements of multilayer films, respectively.

2. Experimental Section

The graphene oxide films were deposited on SiO_2/Si(100) substrates from an aqueous solution of graphene oxide platelets. The nominal thickness of the SiO_2 overlayers was 300 nm. The graphene oxide solutions were formed by exfoliation of graphite oxide, which was produced by chemical oxidation of graphite using the modified Hummers method.[13] Two different methods are used by our group to exfoliate the platelets: sonication and slow-stirring. The exfoliation is performed on samples with a concentration of 1 mg of graphite oxide per 1 mL of deionized water. The sonicated platelets are exfoliated using a 150 W ultrasonic bath, where the signature for complete exfoliation into single-layer graphene oxide platelets is a conversion of the suspension from opaque to clear, which typically takes about 30 min. The platelets produced by this method have an average lateral size of ~0.5 μm.[29] Since it is difficult to grow patterned electrodes onto platelets this small, the method of slow-stirring, which produces platelets with a much larger lateral size, was used for the measurements presented in this study. For the exfoliation of the slow-stirred platelets, the graphite oxide/water mixture is stirred with a Teflon-coated stir bar for about a week, which only results in partial exfoliation of the platelets. Therefore, the suspension is sedimented, and the clear liquid
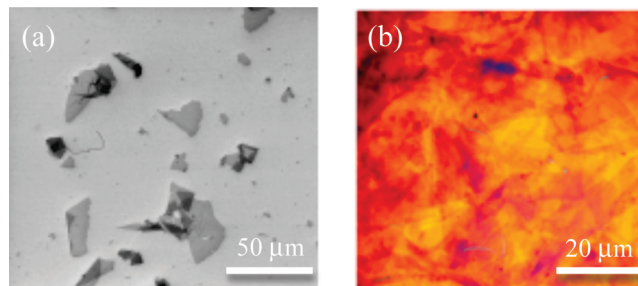
Figure 2. (a) SEM image of submonolayer coverage of slow-stirred graphene oxide platelets deposited on a Si(100) substrate and (b) optical image of a ~9 ML thick film composed of single-layer graphene oxide platelets deposited on 300 nm SiO_2/Si(100).
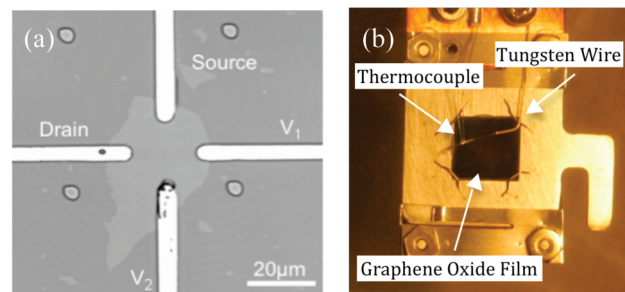

Figure 3. (a) Optical image of patterned electrodes on an individual graphene oxide platelet and (b) sample mounting arrangement for TPD measurements of multilayer graphene oxide films.

above, which contains large platelets of single-layer graphene oxide, is used. This technique results in graphene oxide platelets with an average lateral size of ~10 μm. A scanning electron microscope (SEM) image of a submonolayer coverage of slow-stirred platelets on a Si(100) substrate is shown in Figure 2a.

For the resistivity measurements, single-layer graphene oxide films were formed by applying a droplet of the slow-stirred graphene oxide solution on the substrate followed by dispersion of the droplet by blowing with dry N_2 gas. The electrical resistivity measurements were performed using a differential four-point probe technique.[30,31] The electrodes were formed by deposition of a Au film with a Cr buffer layer using a high-vacuum, e-beam, evaporation system and a photolithographic technique. The Si substrates were mounted on a sample holder stage and heating of the single-layer platelets was performed inside the SEM chamber (Nova NanoSEM600, FEI Co.), which has a base pressure of 1 × 10⁻⁶ Torr. Temperature measurements were performed with a thermistor that sits below the sample (Figure 1a). To correct for the temperature differential between the front surface of the Si substrate and the bottom of the sample holder where the thermistor is located, a calibration curve was measured with a thermocouple attached to the front of a blank substrate. Further details of the resistivity measurement procedure have been described in previous publications.[4,11] A confocal microscope image of a single-layer graphene oxide platelet with patterned electrodes is shown in Figure 3a.

For the TPD measurements, depositing several droplets on the substrate and letting the suspension dry in air resulted in multilayer films (Figure 2b). The average thickness of the films grown from slow-stirred platelets was measured to be 8.5 ± 0.6 nm using ellipsometry (MV-2000, JA Woollam). AFM measurements of graphene oxide films grown using this technique reveal an individual step height of 1 nm for each platelet; therefore, the average thickness of the graphene oxide films grown from slow-stirred platelets is ~9 monolayers (ML).
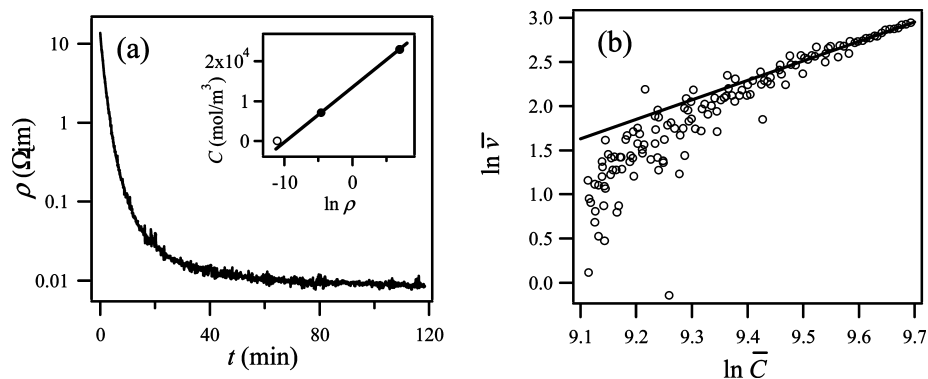
Figure 4. (a) Electrical resistivity of an individual graphene oxide sheet reduced at a fixed temperature of 200 °C (inset: scaling of electrical resistivity to molar concentration of oxygen fraction, where graphene oxide before and after reduction is marked with filled circles (●) and amorphous carbon ($\rho_C = 1.6 \times 10^{-5}$ $\Omega \cdot m$[35]) is marked with an open circle (○)) and (b) the relation between mean molar concentration $\ln \bar{C}$ and mean reduction velocity $\ln \bar{v}$, with line of slope $n = 2.2$ fit to the high concentration region of plot.

The TPD measurements were performed using a 200 amu, quadrupole, residual gas analyzer (RGA) with electron multiplier (Hiden HAL 201) mounted in a UHV chamber with a base pressure of 5×10^{-11} Torr. The ionizer section of the RGA was fitted with a shroud and a collimator that have 6 mm holes in their centers to allow detection of gas molecules evolving from the surface of the graphene oxide film while preventing the detection of molecules desorbing from other areas of the sample holder assembly. The samples (13 mm × 13 mm) were mounted on a molybdenum plate with a hole (9.5 mm diameter) in the center to allow radiative heating of the sample from a tungsten filament mounted behind the sample holder. Linear heating rates were generated using a computer controlled proportional feedback control system. Since our TPD measurements indicate that graphene oxide begins to decompose at temperatures as low as 70 °C, a load lock was used for insertion of samples into the UHV chamber, which permitted the transfer of samples into the chamber without bake out, which would cause partial decomposition of the oxide. To allow temperature measurements of the graphene oxide films, a custom sliding thermocouple mount was used. The sliding contact consists of a chromel−alumel thermocouple (0.13 mm diameter leads) spot-welded to the apex of a bent tungsten wire (0.25 mm diameter), which makes direct contact with the front of the sample. The sample holder assembly with sliding thermocouple mount is shown in Figure 3b. The primary drawback of this measuring technique is that the temperature measured by the thermocouple at the point of contact will be less than that of the rest of the graphene oxide film because of heat transfer along the thermocouple leads and tungsten spring. To estimate the amount of temperature offset, a tantalum plate was mounted on the sample holder and heated until it just began to glow, resulting in a measured thermocouple temperature of 475 °C. By heating the plate further until the region near the contact point of the tungsten wire began to glow, a temperature of 600 °C was measured, which gives a temperature offset of 125 at 475 °C. A linear offset was applied to all of the temperature measurements to compensate for this effect. Although the repeatability of the TPD profiles for similar heating rates was found to be within 2 or 3 °C of each other, the absolute temperature at T_M is estimated to be accurate to only ±20 °C.

3. Results

3.1. Temperature Dependent Resistivity Measurements.
The highest temperature used for the reduction of the single-layer graphene oxide in high vacuum (∼10^{-6} Torr) was 200 °C. The average value of the resistivity of five different samples after thermal treatment at this temperature was $2 \pm 0.7 \times 10^{-2}$ $\Omega \cdot m$, which is much higher than the value for graphite (1 × 10^{-5} $\Omega \cdot m$).[32] There are two primary reasons for this. Previous XPS measurements of the thermal reduction of graphene oxide provide evidence that a temperature much higher than 200 °C is needed to completely remove all or almost all oxygen from the surface.[26] On the basis of elemental analysis by XPS of similarly prepared thin multilayer films of graphene oxide, the C/O ratio of "as prepared" graphene oxide is 3:1 and is reduced down to 9:1 by heating to 500 °C in UHV.[26] In addition, the TPD measurements detect a loss of carbon during the decomposition process (CO_2 and CO). Therefore, the reduced graphene oxide is expected to be highly defective, resulting in additional scattering of charge carriers within the film.

Since there is a strong correlation between the electrical resistivity and stoichiometry of the material, the resistivity can be used to determine the concentration of oxygen in the material. For an intrinsic semiconductor, the temperature dependence of the carrier concentration is given by

$$\eta_i = \sqrt{N_c N_v} \exp\left(-\frac{E_g}{2k_B T}\right) \tag{1}$$

where E_g is the band gap, k_B is the Boltzmann constant, and N_c and N_v are the effective density of states at the bottom of the conduction band and the top of the valence band, respectively. Since graphene oxide is a nonstoichiometric semiconducting compound, it is reasonable to assume that over a finite range of concentrations its band gap should depend linearly on the molar oxygen concentration ($E_g \propto C$). In fact, recent theoretical studies of the dependence of the electrical properties of graphene oxide on the oxygen to carbon ratio predict a linear increase in band gap as the oxygen concentration increases for graphene oxide modeled as being composed of epoxide and hydroxyl groups.[33,34] Since the resistivity is inversely proportional to the carrier concentration, the change in molar oxygen concentration should depend on the difference in natural logarithms of the resistivities

$$C - C_f = p(\ln \rho - \ln \rho_f) \tag{2}$$

where p is a proportionality factor. The time dependence of the resistivity at 200 °C of a single-layer graphene oxide film is shown

Reduction Kinetics of Graphene Oxide

J. Phys. Chem. C, Vol. 113, No. 43, 2009 **18483**
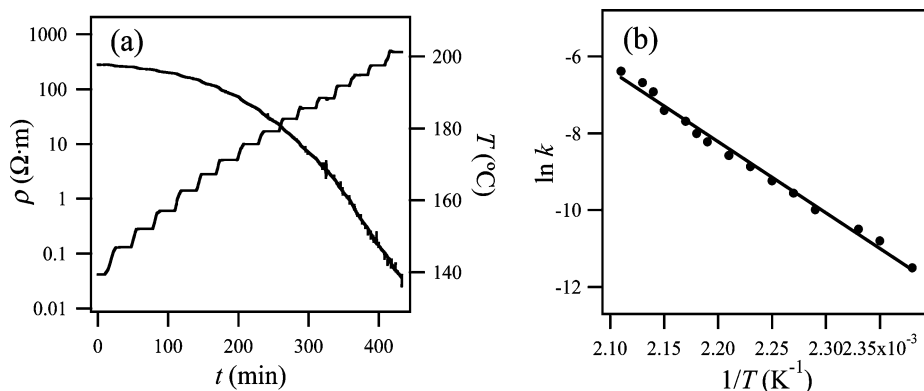
Figure 5. (a) Electrical resistivity and the temperature profile of an individual graphene oxide sheet during reduction using a 5 K stepwise change in temperature and (b) an Arrhenius plot from the rate constants, where the slope of the plot revealed an activation energy of 37 ± 1 kcal/mol.

in Figure 4a, where the final resistivity, ρ_f, is found to be 1×10^{-2} $\Omega \cdot$m and the initial value of the resistivity before heating was measured to be 1×10^3 $\Omega \cdot$m. In the inset of this figure, the molar concentrations of oxygen for graphene oxide are plotted versus the logarithm of the resistivity (filled circles). The molar concentrations are calculated on the basis of the assumption that the atomic carbon-to-carbon distance in the hexagonal structure of graphene oxide is $a = 0.142$ nm and the thickness of graphene oxide is $d = 1$ nm. The number of atoms in the hexagonal unit cell is divided by the volume ($V = 3\sqrt{3}/2a^2d$), which results in a concentration at the beginning stage of 2.3×10^4 mol/m³ and a value at the final stage of 7.1×10^3 mol/m³.[26]

In reaction kinetics, the reaction velocity (v) is related to the nth power of the concentration of reactant ($v = k[C]^n$), where k is the rate constant and n is termed the order of the reaction. The reaction velocity is the rate of change of the concentration, $v = -dC/dt$, for the nonstoichiometric compound. By plotting $\ln v$ versus $\ln C$, the reaction order can be determined from the slope of the curve. As shown in Figure 4b for a single-layer graphene oxide sample annealed at 200 °C, the reaction order is estimated to be 2.2 over most of the range of oxygen concentrations. Once the reaction order is estimated, the time dependence of the rate constant can be determined using the oxygen concentrations estimated from eq 2.

The temperature dependence of the rate constant for graphene oxide is assumed to follow an Arrhenius dependence

$$k = A \exp\left(-\frac{E_a}{RT}\right) \qquad (3)$$

where A is the pre-exponential factor, E_a is the Arrhenius activation energy, and R is the gas constant. Since the exact pathway for decomposition is unknown, the Arrhenius activation energy is interpreted as the energy barrier for the process of decomposition of the oxide and followed by formation of the desorption products. To obtain the effect of temperature on the rate constant, the resistivity of a single-layer graphene oxide film was monitored using a 5 K stepwise increase in the temperature as shown in Figure 5a. The temperature range was carefully chosen for a relatively slow reduction at the beginning temperature so that a wide range of temperatures could be utilized before saturation occurs. To determine E_a, the natural logarithm of the rate constant is plotted versus inverse temperature as shown in Figure 5b. The slope of the curve is the activation energy divided by the gas constant, which results in an activation energy of 37 ± 1 kcal/mol (1.6 eV/molecule) for the single-layer graphene oxide platelets. One aspect of the

determination of the activation energy that should be considered is the assumption that the band gap of graphene oxide depends linearly on the oxygen content. Although the deviation from a linear behavior has not been directly measured, the good fit of the data to a linear curve (Figure 5b) provides indirect evidence that this is a valid assumption over the range of reductions measured in this study.

3.2. Temperature Programmed Desorption. Attempts were made to measure TPD spectra of dispersed single-layer platelets prepared in a similar way to the samples used in the temperature-dependent resistivity measurements. However, the partial pressures of H_2O, CO_2, and CO from the desorbing molecules were generally lower than the partial pressures of the corresponding residual gases in the UHV chamber. To increase the signal-to-noise level of the TPD experiment, graphene oxide films composed of multiple layers of single-layer-thick platelets were used. The TPD spectra taken at a heating rate of $\beta = 30$ °C/min for a mass to charge ratio of $m/z = 18$, 28, 32, and 44, which correspond to the detection of H_2O, CO, O_2, and CO_2, are shown in Figure 6a for an ∼9 ML film. To compensate for the difference in ionization efficiency of each molecular species by the RGA, the measured partial pressures have been divided by the corresponding relative sensitivity of each molecular species.[36] Since CO is a cracking fragment of CO_2 with a relative percentage of 8%,[36] this component has been subtracted from the measured intensity of the $m/z = 28$ partial pressure. To determine the relative amount of each desorbing species from films produced from the slow-stirred graphene oxide platelets, the areas under the partial pressure versus time curves were calculated and are presented in Table 1. The data for the films of slow-stirred platelets were averaged over five samples. As can be seen from the data presented in Figure 6a and Table 1, the primary desorption component of the samples is H_2O, followed by CO_2 and CO. The large H_2O component is not unexpected since the films were deposited from aqueous suspensions, and interlamellar H_2O is known to be an integral part of the structure of graphite oxide as well as 'graphene oxide paper'.[37] A comparison of the CO_2/CO area ratio for slow-stirred samples provides a value of 1.9.

To determine if isolated OH groups or O atoms are desorbing during the decomposition of the graphene oxide, TPD spectra for $m/z = 17$ and 16 were taken. Since the ionization of H_2O in the RGA also produces some OH (21%) and O (2%) and the ionization of CO_2 and CO also produces some O (9% and 2%, respectively), the measured spectra for $m/z = 17$ and 16 must be corrected for these cracking components. TPD spectra for $m/z = 17$, 16, and 15 after the cracking components from H_2O, CO_2, and CO were subtracted are shown in Figure 6b. The m/z
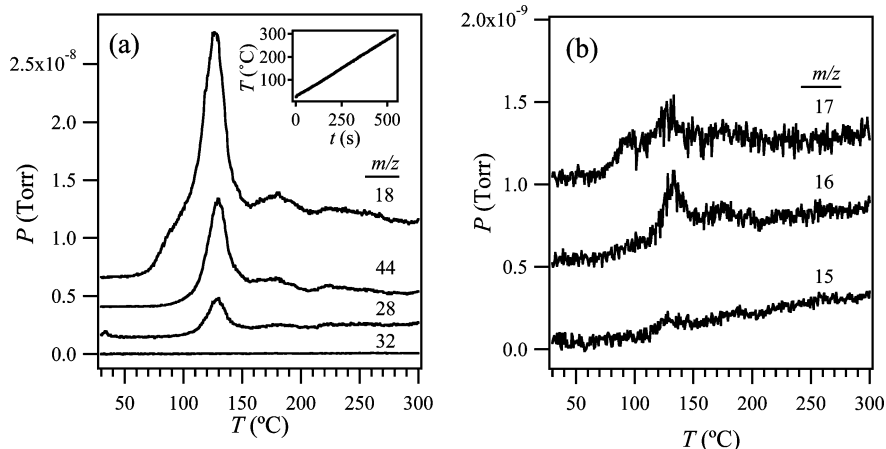
Figure 6. TPD spectra taken at a heating rate of $\beta = 30$ °C/min for ~9 ML thick film of "slow-stirred" graphene oxide (a) for $m/z = 18$, 28, 32 and 44, where the inset shows the measured heating rate of the sample, and (b) for $m/z = 17$, 16, and 15.

TABLE 1: Areas under Partial Pressure Versus Time Curves for Films of Graphene Oxide

m/z	$A_{slow-stirred}$ (Torr·s)
18	$2.3 \pm 0.4 \times 10^{-6}$
28	$5.3 \pm 0.9 \times 10^{-7}$
32	$1.4 \pm 0.4 \times 10^{-8}$
44	$1.0 \pm 0.1 \times 10^{-6}$

= 17 spectrum shows only a small broad peak centered at 130 °C, which is most likely the result of a slight deviation of the cracking fraction of OH from H_2O for our RGA from the standard value of 21%. However, there is a peak for $m/z = 16$ that is centered at 130 °C, which is probably due to methane (CH_4) desorption since there is also a small peak for $m/z = 15$ at this same temperature, which would correspond to the cracking component CH_3.

The activation energies of the films composed of slow-stirred platelets of graphene oxide can be measured with TPD if one assumes an Arrhenius dependence for the probability of desorption. Since the partial pressure of each decomposition product is proportional to the rate of desorption $R_{des} = -d\theta/dt$ of that species from the surface of the film, where θ is the instantaneous coverage, the desorption rate can be written as

$$-\frac{d\theta}{dt} = \nu\theta^n \exp\left(\frac{-E_a}{RT}\right) \qquad (4)$$

where ν is the frequency factor.[38] If the sample is heated at a constant rate $\beta = dT/dt$, the rate of change of coverage can be written as

$$\frac{d\theta}{dT} = -\frac{\nu\theta^n}{\beta} \exp\left(\frac{-E_a}{RT}\right) \qquad (5)$$

By taking the derivative with respect to temperature of eq 5 and setting it equal to zero, the temperature, T_M, at which the maximum of the partial pressure occurs for a sample heated at constant rate β can be found.[39] This results in the expression

$$\ln\left(\frac{T_M^2}{\beta}\right) = \frac{E_a}{R}\frac{1}{T_M} - \ln\left(\frac{n\nu R\theta^{n-1}}{E_a}\right) \qquad (6)$$

The results of the resistivity measurements of single-layer graphene oxide indicate that the order of the decomposition kinetics is ~2;
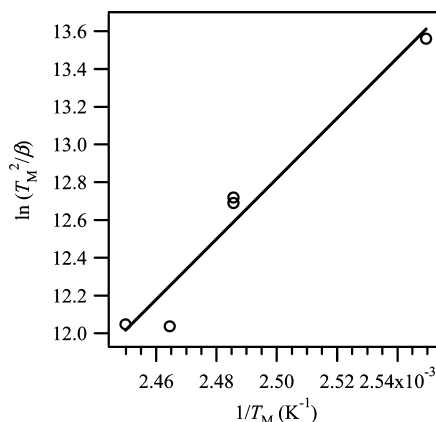
Figure 7. Plot of $\ln(T_M^2/\beta)$ versus $1/T_M$ for CO_2 desorption measured with heating rates of 12, 30, and 59 °C/min for ~9 ML thick films of "slow-stirred" graphene oxide, where the slope of the plot revealed an activation energy of 32 ± 4 kcal/mol.

therefore, the value of T_M will depend on the coverage θ for a fixed heating rate β. Since the multilayer graphene oxide films in this study are all prepared from the same graphene oxide suspension of slow-stirred source material, the relative coverage of oxygen and hydrogen in the platelets of the films should be the same for each sample. A plot of $\ln(T_M^2/\beta)$ versus $1/T_M$ for CO_2 desorption measured with heating rates of 12, 30, and 59 °C/min is shown in Figure 7. The activation energy found from the slope of this curve is 32 ± 4 kcal/mol (1.4 eV/molecule).

4. Discussion

Since it is relatively easy to exfoliate single-layer graphene oxide from graphite oxide, this could be used as a source for nanometer-thick dielectric layers for use in both nanoelectronics and chemical sensor applications. However, the TPD results indicate that the decomposition of graphene oxide begins at the relatively low temperature of 70 °C, which limits applications on the basis of graphene oxide to approximately room temperature and below. Another application of graphene oxide that has sparked great interest is the possible use of graphene oxide as a precursor for the formation of single-layer graphene. Ideally, the reduction of graphene oxide would be accomplished by the desorption of the O and OH groups via the formation of O_2 and H_2O, which would leave the carbon backbone of the graphene intact. However, the TPD measurements show almost no O_2 formation and a relatively large amount of CO_2 and CO

Reduction Kinetics of Graphene Oxide

J. Phys. Chem. C, Vol. 113, No. 43, 2009 **18485**

desorbing during the decomposition of the oxide. Since carbon is lost during the reduction process in UHV, the addition of other carbon-containing reactants during the thermal reduction will be needed to regain the electrical and mechanical properties of pristine graphene.

For TPD measurements of gas molecules adsorbed on single-crystal surfaces, multiple desorption peaks are often observed, which results from different binding sites on the surface (on-top, bridge, 3-fold hollow, etc.). For the TPD measurements of graphene oxide, the desorption peaks of H_2O, CO_2, and CO are all observed at the same temperature. Since the reduction of graphene oxide is a decomposition process where some of the carbon backbone is lost, the breaking of carbon–carbon bonds must trigger a change in the local chemical potential that is strong enough to initiate the simultaneous formation of all of the desorption products. A first-order desorption process is associated with the direct desorption of a particular molecular species, whereas a second-order desorption processes involves an intermediate step before desorption. Therefore, the measured value of $n = 2.2$ from the temperature-dependent resistivity measurements is in general agreement with the expected $n = 2$ desorption kinetics for the decomposition of graphene oxide.

5. Conclusion

The thermal reduction kinetics of graphene oxide have been monitored using temperature-dependent resistivity measurements under high vacuum and using TPD in UHV. The exfoliation of single-layer graphene oxide from graphite oxide has been accomplished by slow-stirring, which produces platelets with an average lateral size of ∼10 μm. The TPD measurements for temperatures up to 300 °C find that the primary desorption components of graphene oxide are H_2O, CO_2, and CO, with only trace amounts of O_2 being detected. The detection of CO_2 and CO provides evidence that carbon is being lost from the graphene backbone of the oxide during the reduction process. The desorption kinetics have been estimated from the temperature-dependent resistivity measurements to be 2.2. For the decomposition of the slow-stirred graphene oxide, activation energies of 37 ± 1 and 32 ± 4 kcal/mol are measured by resistivity measurements on single-layer graphene oxide and TPD measurements of multilayer films, respectively.

References and Notes

(1) Gilje, S.; Han, S.; Wang, M.; Wang, K. L.; Kaner, R. B. A Chemical route to graphene for device applications. *Nano Lett.* **2007**, *7* (11), 3394–3398.

(2) Gomez-Navarro, C.; Thomas Weitz, R. T.; Bittner, A. M.; Scolari, M.; Mews, A.; Burghard, M.; Kern, K. Electronic transport properties of individual chemically reduced graphene oxide sheets. *Nano Lett.* **2007**, *7* (11), 3499–34503.

(3) Si, Y.; Samulski, E. T. Synthesis of water soluble graphen. *Nano Lett.* **2008**, *8* (6), 1679–1682.

(4) Jung, I.; Dikin, D. A.; Park, S.; Cai, W.; Mielke, S. L.; Ruoff, R. S. Effect of water vapor on electrical properties of individual reduced graphene oxide sheets. *J. Phys. Chem. C* **2003**, *112* (51), 20264–20268.

(5) McAllister, M. J.; Li, J. L.; Adamson, D. H.; Schniepp, H. C.; Abdala, A. A.; Liu, J.; Herrera-Alonso, M.; Milius, D. L.; Car, R.; Prud'homme, R. K.; Aksay, I. A. Single sheet functionalized graphene by oxidation and thermal expansion of graphite. *Chem. Mater.* **2007**, *19*, 4396–4404.

(6) Stankovich, S.; Dikin, D. A.; Piner, R. D.; Kohlhaas, K. A.; Kleinhammes, A.; Jia, Y.; Wu, Y.; Nguyen, S. T.; Ruoff, R. S. Synthesis of graphene-based nanosheets via chemical reduction of exfoliated graphite oxide. *Carbon* **2007**, *45*, 1558–1565.

(7) Paci, J. T.; Belytschko, T.; Schatz, G. C. Computational studies of the structure, behavior upon heating, and mechanical properties of graphite oxide. *J. Phys. Chem. C* **2007**, *111*, 18099–18111.

(8) Kudin, K. N.; Ozbas, B.; Schniepp, H. C.; Prud'homme, R. K.; Aksay, I. A.; Car, R. Raman spectra of graphite oxide and functionalized graphene sheets. *Nano Lett.* **2008**, *8* (1), 36–41.

(9) Becerril, H. A.; Mao, J.; Liu, Z.; Stoltenberg, R.; Bao, Z.; Chen, Y. Evaluation of solution-processed reduced graphene oxide films as transparent conductors. *ACS Nano* **2008**, *2* (3), 463–470.

(10) Eda, G.; Fanchini, G.; Chhowalla, M. Large-area Ultrathin films of reduced graphene oxide as transparent and flexible electronic material. *Nat. Nanotechnol.* **2008**, *3*, 270–274.

(11) Jung, I.; Dikin, D. A.; Piner, R. D.; Ruoff, R. S. Tunable electrical conductivity of individual graphene oxide sheets reduced at "low" temperatures. *Nano Lett.* **2008**, *8* (12), 4283–4287.

(12) Brodie, B. C. Sur le poids atomique du graphite. *Ann. Chim. Phys.* **1860**, *59*, 466–472.

(13) Hummers, W. S., Jr.; Offeman, R. E. Preparation of graphitic oxide. *J. Am. Chem. Soc.* **1958**, *80*, 1339.

(14) Staudenmaier, L. Verfahren zur Darstellung der Graphitsäure. *Ber. Dtsch. Chem. Ges.* **1898**, *31*, 1481–1499.

(15) Stankovich, S.; Piner, R. D.; Chen, X.; Wu, N.; Nguyen, S. T.; Ruoff, R. S. Stable aqueous dispersions of graphitic nanoplatelets via reduction of exfoliated graphite oxide in the presence of poly(sodium 4-styrenesulfonate). *J. Mater. Chem.* **2006**, *16* (2), 155–156.

(16) Stankovich, S.; Piner, R. D.; Nguyen, S. T.; Ruoff, R. S. Synthesis and exfoliation of isocyanate-treated graphene oxide nanoplatelets. *Carbon* **2006**, *44* (15), 3342–3347.

(17) Szabo, T.; Berkesi, O.; Forgo, P.; Josepovits, K.; Sanakis, Y.; Petridis, D.; Dékány, I. Evolution of surface functional groups in a series of progressively oxidized graphite oxides. *Chem. Mater.* **2006**, *18*, 2740–2749.

(18) Hofmann, U.; Holst, R. Über die Säurenatur und die Methylierung von Graphitoxyd. *Ber. Dtsch. Chem. Ges.* **1939**, *72*, 754–771.

(19) Lerf, A.; He, H.; Forster, M.; Klinowski, J. Structure of graphite oxide revisited. *J. Phys. Chem. B* **1998**, *102* (23), 4477–4482.

(20) Ruess, G. Über das Graphitoxyhydroxyd (Graphitoxyd). *Monatsh. Chem.* **1946**, *76*, 381–417.

(21) Scholz, W.; Boehm, H. P. Untersuchungen am Graphitoxyd. *Z. Anorg. Allg. Chem.* **1969**, *369*, 327–340.

(22) Nakajima, T.; Matsuo, Y. Formation process and structure of graphite oxide. *Carbon* **1988**, *32* (3), 469–475.

(23) Cai, W.; Piner, R. D.; Stadermann, F. J.; Park, S.; Shaibat, M. A.; Ishii, Y.; Yang, D.; Velamakanni, A.; An, S. J.; Stoller, M.; An, J.; Chen, D.; Ruoff, R. S. Synthesis and solid-state NMR structural characterization of 13C-labeled graphite oxide. *Science* **2008**, *321*, 1815–1817.

(24) Scholtz, W.; Boehm, H.-P. Die thermische Zersetzung von Graphitoxyd. *Naturwissenschaften* **1963**, *51* (7), 160.

(25) Schniepp, H. C.; Li, J. L.; McAllister, M. J.; Sai, H.; Herra-Alonso, M.; Adamson, D. H.; Prud'homme, R. K.; Car, R.; Saville, D. A.; Aksay, A. Functionalized single graphene sheets derived from splitting graphite oxide. *Phys. Chem. B* **2006**, *110*, 8535–8539.

(26) Yang, D.; Velamakanni, A.; Bozoklub, G.; Park, S.; Stoller, M.; Piner, R. D.; Stankovich, S.; Jung, I.; Field, D. A.; Ventrice, C. A., Jr.; Ruoff, R. S. Chemical analysis of graphene oxide films after heat and chemical treatments by X-ray photoelectron and micro-raman spectroscopy. *Carbon* **2009**, *47*, 145–152.

(27) Mattevi, C.; Eda, G.; Agnoli, S.; Miller, S.; Mkhoyan, K. A.; Celik, O.; Mastrogiovanni, D.; Granozzi, G.; Garfunkel, E.; Chhowalla, M. Evolution of electrical, chemical, and structural properties of transparent and conducting chemically derived graphene thin films. *Adv. Funct. Mater.* **2009**, *19*, 2577–2583.

(28) Boehm, H.-P. Surface chemical characterization of carbons from adsorption studies. In *Adsorption by carbons*; Elsevier: Amsterdam, 2008; pp 301−27.

(29) Fan, F. R.; Park, S.; Zhu, Y.; Ruoff, R. S.; Bard, A. J. Electrogenerated chemiluminescence of partially oxidized highly oriented pyrolytic graphite surfaces and of graphene oxide nanoparticles. *J. Am. Chem. Soc.* **2008**, *131*, 937–939.

(30) Van der Pauw, L. J. A method of measuring specific resistivity and Hall effect of discs of arbitrary shape. *Philips Res. Reports* **1958**, *13*, 1–9.

(31) Van der Pauw, L. J. A method of measuring the resistivity and Hall coefficient on lamellae of arbitrary shape. *Philips Tech. Rev.* **1958**, *20*, 220–224.

(32) Powell, R. L.; Childs, G. E. *American institute of physics handbook*, 3rd ed.; McGraw-Hill: Dallas, 1972; pp 142−160.

(33) Boukhvalov, D. W.; Katsnelson, M. I. Modeling of graphite oxide. *J. A. Chem. Soc.* **2008**, *130*, 10697–10701.

(34) Yan, J.-A.; Xian, L.; Chou, M. Y. Structural and electronic properties of oxidized graphene. *Phys. Rev. Lett.* **2009**, *103*, 086802.

(35) Stransfield, A. *The electric furnace: its construction, operation and uses*; McGraw-Hill: New York, 1914; p 89.

(36) Hiden Analytical (http://www.hidenanalytical.com/index.php/en/cracking-patterns).

(37) Dikin, D. A.; Stankovich, S.; Zimney, E. J.; Piner, R. D.; Dommett, H. B.; Evmenenko, G.; Nguyen, S. T.; Ruoff, S. R. Preparation and characterization of graphene oxide paper. *Nature* **2007**, *448*, 457–460.

(38) Polanyi, M.; Wigner, E. Bildung und Zerfall von Molekülen. *Z. Phys.* **1925**, *33* (1), 429–434.

(39) Redhead, P. A. Thermal desorption of gases. *Vacuum* **1962**, *12*, 203–211.